Relationship between fill factor and light intensity in solar cells based on organic disordered semiconductors: The role of tail states

Biao Xiao[1], Philip Calado[2], Roderick C. I. MacKenzie[3], Thomas Kirchartz[4,5], Jun Yan[2,*], Jenny Nelson[2]

[1]Key Laboratory of Optoelectronic Chemical Materials and Devices, Ministry of Education, Flexible Display Materials and Technology Co-Innovation Centre of Hubei Province, School of Chemical and Environmental Engineering, Jianghan University, Wuhan, 430056, China.

[2]Department of Physics and Centre for Plastic Electronics, Imperial College London, SW7 2AZ, London, United Kingdom.

[3]Faculty of Engineering, University of Nottingham, University Park, NG7 2RD Nottingham, United Kingdom.

[4]IEK5-Photovoltaics, Forschungszentrum Jülich, 52425 Jülich, Germany

[5]Faculty of Engineering and CENIDE, University of Duisburg-Essen, Carl-Benz-Str. 199, 47057 Duisburg, Germany

Corresponding E-mail: j.yan17@imperial.ac.uk

ABSTRACT

The origin of the relationship between fill factor and light intensity (*FF-I*) in organic disordered-semiconductor based solar cells is studied. An analytical model describing the balance between transport and recombination of charge carriers, parameterized with a factor, Γ_m, is introduced to understand the *FF-I* relation where higher values of Γ_m correlate to larger *FF*. Comparing the effects of direct and tail state mediated recombination on the *FF-I* plot, we find that for low mobility systems direct recombination with constant transport mobility can only deliver a negative dependence of $\Gamma_{m,dir}$ on light intensity. By contrast, tail state mediated recombination with trapping and de-trapping processes can produce a positive $\Gamma_{m,t}\ vs. Sun$ dependency. The analytical model is validated by numerical drift-diffusion simulations. To further validate our model, two material systems that show opposite *FF-I* behaviour are studied: PTB7-Th:$PC_{71}BM$ devices show a negative *FF-I* relation while PTB7-Th:O-IDTBR devices show a positive correlation. Optoelectronic measurements show that the O-IDTBR device presents a higher ideality factor, stronger trapping and de-trapping behaviour, and a higher density of trap states, relative to the $PC_{71}BM$ device, supporting the theoretical model. This work provides a comprehensive understanding of the correlation between *FF* and light intensity for disordered semiconductor based solar cells.

I. INTRODUCTION

Organic semiconductors [1–5] are widely studied material systems for photovoltaic applications, due to their ease of processing, chemical tunability, low cost, flexibility, and low weight. However, as the materials are intrinsically disordered, they often have lower mobilities and increased density of trap states relative to more ordered semiconductors [6]. Consequently, when used as active materials for thin-film photovoltaics, the competition between charge carrier extraction and charge recombination is a key concern affecting the magnitude of the photogenerated current density at operating point. These losses often result in a reduction in the current density-voltage (*J-V*) curve fill factor (FF) of devices. The FF is determined by the ratio between maximum power generated, which is the product of the current density (J_m) and voltage (V_m) at maximum power point (MPP), and the product of short circuit current density (J_{sc}) with the open circuit voltage (V_{oc}), such that [7]

$$FF = \frac{J_m V_m}{J_{sc} V_{oc}}. (1)$$

The performance of a photovoltaic device is therefore related to FF through $\eta = J_{sc} V_{oc} FF / P_s$, where η is the power conversion efficiency, and P_s is the incident light power density [7]. Therefore, to maximize the η, a high FF is required.

Measuring the current voltage characteristics at one sun characterizes the devices under the standard solar illumination. Understanding device responses at lower light intensities is important for determining annual energy conversion yields and in particular for indoor photovoltaics. [8,9] Additionally, studying light intensity-dependent performance can provide insight into loss mechanisms in devices. [10,11] However, the majority of studies based on light intensity-dependent performance measurements are focused on either V_{oc} [10,12,13] or

J_{sc} [10,11,14]. Only a limited number have investigated *FF* [15] owing to the difficulty in describing its physical origins and accounting for the many factors that contribute to it.

In most of those studies based on organic solar cells, *FF* has been shown to decrease with increasing light intensity. [16–21] A small number of studies, however, have shown the reverse, namely that *FF* increases with light intensity for intensities below one sun. [15,22] The first type of behaviour has been rationalized by either a super-linear increase in the bimolecular recombination rate with charge density and hence light intensity, [21] or series resistive effects. [23] In the second type of behaviour, where *FF* increases with increasing light intensity, the reasons are less clear. Researchers have proposed that the leakage current due to low shunt resistance in organic solar cells (OSCs) [15,23] controls the *FF* under low light intensity, resulting in a reduction of *FF* at very low light intensities (less than 10^{-5} Sun). [23] [15] However, the leakage current cannot easily be differentiated from the dark saturation current [24,25] making it difficult to extract the key information solely from the shunt resistance values measured using the dark current. At present no complete model exists to explain these two types of behaviour.

The *FF* of low mobility semiconductor-based solar cells has been correlated to the competition between charge recombination and charge extraction [26,27] with the earliest study dating back to 1932 by Hecht. [28] Bartesaghi et al. [29] adapted this concept and applied it to organic solar cells successfully. The concept was later used to derive analytical expressions for the *J-V* curve of a low mobility diode [30] and was extended [31] to take recombination mechanisms, space-charge effects, and contacts into account. All of these models have been successfully applied to OSCs under standard solar illumination (1 Sun). At lower light intensities however, the carrier-density dependence of transport and recombination processes becomes more important and is expected to affect the *FF-I* relation. Considering the disordered nature of OSCs, caused by the distribution of conjugation lengths, disorder in conformation, and crystallinity, etc., the extended density of electronic states (DOS) and the associated dispersive charge transport and recombination processes must be included in any analysis that aims to explain the behavior of the *FF* over orders of magnitude in light intensity.

In this paper, we derive an analytical model to describe the correlation between *FF* and light intensity in organic disordered semiconductor-based solar cells. We consider separately the effects of direct and trap-mediated recombination on the *FF-I* plot. Our analytical models are verified using a more complex one-dimensional numerical drift-diffusion simulation based on the General Purpose Photovoltaic Device Model (gpvdm) software. [32,33] Our results suggest that, for low mobility systems, devices that are limited by direct recombination always show negative dependence of *FF* on light intensity, while devices with tail states can show the opposite behavior. In order to test the proposed model we study two different types of organic blend device that showed different *FF-I* relationships, one based on a poly[4,8-bis(5-(2-ethylhexyl)thiophen-2-yl)benzo[1,2-b;4,5-b']dithiophene-2,6-diyl-alt-(4-(2-ethylhexyl)-3-fluorothieno[3,4-b]thiophene-)-2-carboxylate-2-6-diyl)] (PTB7-Th) [34] : [6,6]-Phenyl-C71-butyric acid methyl ester ($PC_{71}BM$) absorber layer and the other (PTB7-Th:O-IDTBR) using the non-fullerene acceptor (5Z,5′Z)-5,5′-(((4,4,9,9-tetraoctyl-4,9-dihydro-s-indaceno[1,2-b:5,6-b′] dithiophene-2,7-diyl) bis (benzo [c] [1,2,5] thiadiazole-7,4-diyl)) bis (methanylylidene)) bis (3-ethyl-2-thioxothiazolidin-4-one) (O-IDTBR) [35,36] instead of the fullerene $PC_{71}BM$. The theoretical analysis is supported by experimental estimation of the trap states in the two device types. The PTB7-Th:O-IDTBR device is shown to have a higher ideality factor, stronger trapping and de-trapping behaviour, and higher trap density than the $PC_{71}BM$ device, leading to a positive *FF-I* relation as opposed to the negative relation shown in the $PC_{71}BM$ device.

II. THEORY AND MODEL

The FF of a classical inorganic solar cell depends on the two resistive elements of the standard equivalent circuit of a solar cell, namely the series and parallel resistance (R_s and R_p). [37] In addition, the voltage dependence of the recombination current J_{rec} matters. This voltage dependence is approximately exponential, scaling with $J_{rec} \sim \exp\,[qV/(n_{id}k_bT)]$, where k_bT/q is the thermal voltage and n_{id} is the ideality factor that provides information about the dominant recombination mechanism. [38,39] Several studies have discussed how resistive effects and recombination mechanisms change the relationship between fill factor and light intensity using diode equation, which we will call the *FF-I* relationship [40,41]. In the absence of resistive effects and recombination through trap states, the *FF* should depend on light intensity in a similar way to V_{oc} , i.e. increased light intensity results in a higher V_{oc} and *FF*. [37,40] Series resistance losses, however, increase with increasing current density and may cause an associated decrease of the *FF* with higher light intensities. The addition of trap recombination or shunt resistances may result in an increase of the *FF* with light intensity. [40] However, these insights are based on the standard equivalent circuit model of a solar cell under illumination, and do not account for disorder or inefficient charge collection.

In the case of disordered organic or inorganic absorber materials, low mobilities are generally undesirable. Hence, to compensate for the effects of low mobilities, the device design of disordered organic or inorganic materials is typically chosen such that the absorber layer is fully or nearly-fully depleted. For low mobility-lifetime products, the wide field-bearing depletion zone helps to achieve efficient charge extraction, relative to a partially depleted design [42]. The electric field in a fully depleted organic solar cells is approximately given by $(V_{bi} - V)/d$, where V_{bi} is the built-in potential, V is the applied voltage and d is the active layer thickness. Because the electric field affects the probability of charge collection [26,27], the recombination current can be voltage and illumination dependent, as opposed to the standard equivalent circuit description of a solar cell, and consequently, the superposition principle [43] can no longer be applied. Instead, a range of different effects may influence the light intensity dependence of the fill factor. These have been described variously as light intensity- and voltage-dependent photocurrents, [26,27] recombination currents, [21] internal series resistances, [44] or even ideality factors, [45] all of which may modify the device current-voltage curve.

Previous modelling studies [29–31] had great success in understanding the limitations on *FF* under 1 Sun. For example, a study by Koster and co-workers [29] introduced a factor, θ, representing the recombination-to-extraction rate at short circuit as a way to quantify collection efficiency and indicate *FF*. This approach is referred to as the Koster Model in this paper. However, previous analyses have not considered the impact of charge carrier density-dependent carrier mobility [46,47] nor have they considered the situation at maximum power point. Thus, an adapted analysis is required to properly model disordered systems with significant densities of tail states.

In the model described herein, we compare cases with and without carrier density-dependent charge transport. We begin by considering two types of recombination present in real-world solar cells (rather than assuming only Langevin-type-second-order recombination [29]):

1) Second-order, direct, free electron-to-free hole recombination with no trap-mediated recombination and constant mobility.

2) First order, trap-mediated recombination and transport as they are often seen as the dominating loss mechanism in OSCs. [33,48–51]

We model a device directly at maximum power point (MPP), under the assumption that V_m is proportional to V_{oc}: This has been validated numerically using gpvdm [32,33] (see Fig. S8 in the Supplemental Material [52]) and is often the case for real-world OSCs. [53] It follows that V_m can be expressed as a constant fraction (w) of V_{oc} ($w < 1$) such that:

$$V_m = wV_{oc}, \qquad (2)$$

We consider uniform absorption profile, and charge transport to be drift-dominated at MPP. We also assume that quasi-Fermi levels are spatially invariant at MPP. We parameterize the model using the *transport-to-recombination* factor at MPP: Γ_m. In the model, we define Γ_m as the ratio between the drift transport (K_{dr}) and recombination (K_{rec}) rate constants (both in the unit of s^{-1}) such that $\Gamma_m = K_{dr}/K_{rec}$. For interest, we compare our approach with that taken by Koster and co-workers [29] in Table S1 in the Supplemental Material [52].

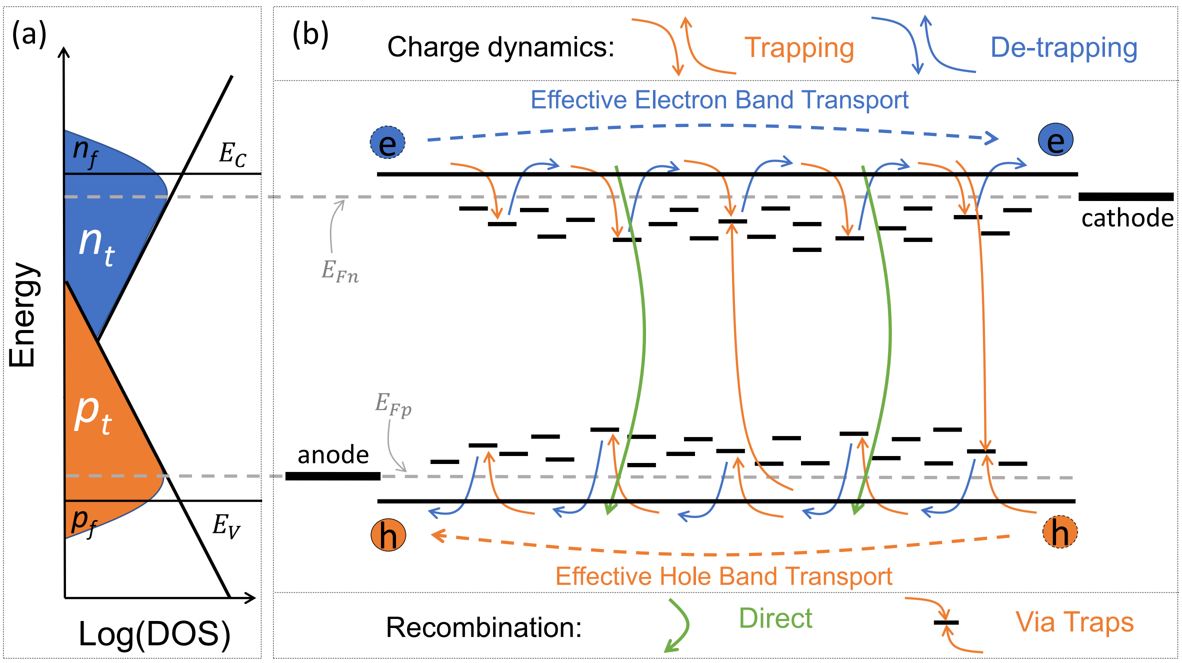

FIG. 1. Illustration of (a) the density of states (DOS), (b) direct recombination, recombination through tail states, and charge transport with multiple trapping and de-trapping processes

assuming an exponential-type density of tail states under flat band condition. This is an assumption that MPP condition is close to flat band condition (OC condition). Free charge densities ($n_{f,}$ $p_{f,}$) and trapped charge densities ($n_{t,}$ $p_{t,}$) are given by the integral of Fermi-Dirac distribution function with the DOS [54]). See Section IV in the Supplemental Material for details [52].

A. A model for devices dominated by direct, second order recombination without tail-states

Direct recombination occurs between a free electron and a free hole, and can be radiative, [55] as illustrated in Fig. 1. For the purpose of this analysis, let us imagine a simple one-dimensional device with symmetric electron and hole distributions, transport and recombination processes. Assuming the averaged quasi-Fermi level splitting across the device equals applied voltage, i.e. $\overline{\Delta E_F} = qV$, the averaged direct recombination rate ($R_{rec,dir}(V)$) can be expressed as a function of the applied voltage (V) via [7]

$$R_{rec,dir}(V) = B_{dir}N_C N_V exp\left(\frac{qV - E_g}{k_B T}\right) = k_{dir}{n_f}^2, (3)$$

where N_C and N_V are the effective density of states for the donor material conduction band and the acceptor material valence band, k_B is the Boltzmann constant, T is the temperature, B_{dir} is the direct recombination coefficient, n_f is the free electron density ($n_f = p_f$), E_g is the effective band gap of the blend set to be equal to the product of the elementary charge (q) and the built-in potential V_{bi}, based on the fact that for most efficient OSCs the contacts match with the HOMO of donor and the LUMO of acceptor. In Eq. (3) we neglect the dark generation term based on the assumption that it is much smaller than the generation rate under the range of illumination intensities of interest. Using Eq. (3), we can relate the recombination rate at MPP to the rate at open circuit (OC), therefore to the light intensity (I), via

$$R_{rec,dir}(V_m) = R_{rec,dir}(V_{oc,dir})exp\left[-\frac{(1-w)qV_{oc,dir}}{k_BT}\right] = C_G I exp\left[-\frac{(1-w)qV_{oc,dir}}{k_BT}\right]. (4)$$

At OC the average volumetric rate of direct recombination $R_{rec,dir}(V_{oc,dir})$ is balanced by the average volumetric generation rate $R_{rec,dir}(V_{oc,dir}) = G = C_G I$, and C_G is the generation rate at 1 Sun illumination. The open-circuit voltage ($V_{oc,dir}$) depends linearly on the effective band gap E_g and logarithmically on light intensity (I) (see Section III in the Supplemental Material for details [52]), via

$$V_{oc,dir} = \frac{E_g}{q} - \frac{k_BT}{q} ln\left(\frac{B_{dir}N_CN_V}{C_G I}\right), (5)$$

With an ideality factor $n_{id,dir}$ of 1, the free charge carrier density at MPP ($n_{f,m}$) can then be expressed as

$$n_{f,m} = \sqrt{\frac{C_G I}{B_{dir}}} exp\left[-\frac{(1-w)qV_{oc,dir}}{2k_BT}\right], (6)$$

We can then describe a pseudo-first order recombination rate ‘constant’ $K_{rec,dir}(n_f)$ (s^{-1}), for which $R_{rec,dir}(V) = K_{rec,dir}(n_f)n_f = n_f/\tau_{dir}$. At MPP, we have

$$K_{rec,dir}(V_m) = \sqrt{B_{dir}C_G I}\, exp\left[-\frac{(1-w)qV_{oc,dir}}{2k_BT}\right]. (7)$$

At MPP, we assume that carrier transport is drift-dominated, which should be valid provided that $V_m < V_{bi}$ and a large enough electric field is maintained. [42] We use the drift rate coefficient (s^{-1}), $K_{dr,dir}(V_m)$ as a proxy for the extraction rate coefficient at MPP to describe the average rate for carriers to drift to the respective contacts: [29]

$$K_{dr,dir}(V_m) = \frac{\mu\left({}^{V_{int,m}}/_{L}\right)}{\left({}^{L}/_{2}\right)} = \frac{2\mu V_{int,m}}{L^2}, (8)$$

Here μ is the constant transport mobility (we assume balanced electron and hole mobilities), L is the layer thickness, and $V_{int,m}$ is the internal electrostatic potential drop across the absorber layer at MPP. The internal voltage $V_{int,m}$ is given by

$$V_{int,m} = V_{bi} - V_m = V_{bi} - wV_{oc,dir}, (9)$$

The transport-to-recombination factor for direct recombination $\Gamma_{m,dir}$ is then

$$\Gamma_{m,dir} = \frac{K_{dr,dir}(V_m)}{K_{rec,dir}(V_m)} = \frac{2\mu}{L^2\sqrt{B_{dir}C_G}} \times \frac{V_{bi} - wV_{oc,dir}}{exp\left[-\frac{(1-w)qV_{oc,dir}}{2k_BT}\right]} \times \frac{1}{\sqrt{I}} \propto \frac{V_{bi} - wV_{oc,dir}}{I^{(w-\frac{1}{2})}}, (10)$$

Since $V_{oc,dir}$ is proportional to the log of the light intensity (I) in Eq. (10), i.e. $V_{oc,dir} \propto ln(I)$, $\Gamma_{m,dir}$ should decrease with light intensity *I* as long as $w > \frac{1}{2}$ is assured (common for practical devices), indicating that direct recombination could only deliver a negative dependence between $\Gamma_{m,dir}$ and I, and hence a negative dependence of *FF* on light intensity. This relationship shows that if the device is limited by direct recombination, *FF* tend to higher values at lower light intensities, as is often reported for high efficiency devices. [18,34] We expect the same result using the Koster model, [29] since in that model the factor θ is proportional to the generation rate (equivalent to light intensity), and the mobility is constant. Therefore, the model devices limited by direct recombination and constant mobility cannot produce a positive *FF-I* correlation.

B. A model for devices dominated by tail state-mediated recombination

Tail state models have often been used to understand the unusual behavior in OSCs [33,48,49] and, as discussed above, are essential to a comprehensive model of devices operating at low light intensity. As we show in this section, only a model including trap-mediated recombination and trap-mediated transport can reproduce the positive FF dependence on light intensity described in the introduction.

This approach is motivated by two key observations in the field of OPVs, i.e. 1) Most devices present ideality factors greater than 1 [56,57]; 2) Langevin-type second-order bimolecular recombination mechanism, that is defined by $R = B_L np$, seldom holds, [58,59] with $B_L = \frac{q}{\varepsilon_0 \varepsilon_r}(\mu_n + \mu_p)$, and ε_0 the vacuum permittivity, and ε_r the relative permittivity of the blend, and μ_n and μ_p are the electron and hole mobility, respectively. These observations lead to the following assumptions:

1) The DOS of organic semiconductors is distributed in energy, and follows an exponential-type distribution function;

2) Charge transport is correlated to charge carrier density through trapping and de-trapping processes, as opposed to the carrier-density independent mobility approximation that is commonly used [29].

Figure 1 is a schematic showing charge carrier occupation and transport in an extended exponential-type DOS based on the concept of multiple trapping and de-trapping. As with the direct recombination analysis, we consider a one-dimensional device with symmetric charge-carrier distributions, transport and recombination. In the trap-mediated recombination model, recombination primarily occurs between free charges and trapped charges. Hence, the average volumetric recombination rate $R_{rec,t}(V)$ can be expressed as [39]

$$R_{rec,t}(V) = B_t n_f p_t \ \ , (11)$$

where B_t is a constant pre-factor, n_f is the free charge carrier density, and p_t is the trapped carrier density and we have neglected the small contribution from dark generation. We assume that the capture coefficients of the conduction band tail from the conduction band are much larger than the capture coefficients of the conduction band tail with the valence band (and vice versa), such that the trapped carriers are in equilibrium with free carriers in each band, i.e. the free and trapped charges in each band share the same quasi Fermi levels. (We note that this assumption is not required in the numerical modelling presented later.) Assuming an identical exponential tail for both conduction and valence bands, the density of trapped (holes) and free carriers (electrons) can be estimated as [60,61]

$$p_t = n_t \approx N_t exp\left(-\frac{\Delta E_F}{E_t}\right), (12a)$$

$$n_f = N_c exp\left(-\frac{\Delta E_F}{k_B T}\right). (12b)$$

Here N_t is the total density of localized trap states determined by $E_t U_t^{exp}$, where U_t^{exp} is the effective density of trap states per unit energy [33] in the unit of m^{-3} eV^{-1} and E_t the characteristic energy of the exponential tail, ΔE_F is the relative position of quasi-Fermi potential to the conduction band for electrons: $\Delta E_F = E_C - E_{Fn} = E_{Fp} - E_V = \frac{1}{2}\left(E_g - qV\right)$, E_C and E_V are the energy of the conduction and valence band edges, respectively. A detailed derivation for free and trapped charge densities, and a discussion on the validity of Eq. (12a) can be found in the Supplemental Material [52]. Using Eq. (12), we can re-write the equation for the hole density in the valence band tail as a function of free electron density in the conduction band:

$$p_t = n_t = N_t \left(\frac{n_f}{N_c}\right)^{k_B T/E_t}, (13)$$

By substituting Eq. (13) into Eq. (11) we obtain:

$$R_{rec,t}(V) = \frac{B_t N_t}{N_c^{\,k_B T/E_t}} n_f^{\left(k_B T/E_t + 1\right)}, (14)$$

So we have the reaction order for free charge carriers, $\Delta = {k_B T}/{E_t} + 1$, as previously derived by Kirchartz & Nelson [39]. Hence, E_t is directly related to the reaction order (Δ) within this framework. The pseudo first order recombination rate coefficient $K_{rec,t}(n_f)$ (s^{-1}) for which $R_{rec,t}(V) = K_{rec,t}(n_f)n_f = n_f/\tau_t$, at MPP is then:

$$K_{rec,t}(V_m) = \frac{B_t N_t}{N_c^{(\Delta-1)}} n_{f,m}^{(\Delta-1)} = \frac{B_t N_t}{N_c^{(\Delta-1)}} n_{f,oc}^{(\Delta-1)} exp\left[-\frac{(\Delta-1)(1-w)qV_{oc,t}}{2k_B T}\right]. (15)$$

Here, the open circuit voltage ($V_{oc,t}$) is given by (see Supplemental Material for details [52])

$$V_{oc,t} = \frac{E_g}{q} - \frac{n_{id,t} kT}{q} \ln\left(\frac{B_t N_t N_c}{C_G I}\right), (16)$$

The ideality factor $n_{id,t}$ is defined by assuming the same characteristic energy for both conduction and valance band (see Supplemental Material for the derivation [52]):

$$n_{id,t} = \frac{2}{1 + \frac{k_B T}{E_t}} = \frac{2}{\Delta}. (17)$$

The free charge density at OC ($n_{f,oc}$) can be directly related to the light intensity (I) based on the fact that at open circuit $R_{rec,t}(V_{oc,t}) = G = C_G I$, through

$$n_{f,oc} = \left[\frac{IC_G N_c{}^{(\Delta-1)}}{B_t N_t}\right]^{1/\Delta}, (18)$$

Hence, the free charge carrier density at MPP ($n_{f,m}$) can be expressed as

$$n_{f,m} = \left[\frac{IC_G N_c{}^{(\Delta-1)}}{B_t N_t}\right]^{1/\Delta} exp\left[-\frac{(1-w)qV_{oc,t}}{2k_B T}\right], (19)$$

Following the same method as Section II.A, we assume that the carrier drift rate coefficient $K_{dr,t}(V_m)$ parameterizes the charge transport rate at MPP for electrons [42]. However, the multiple trapping model requires that we substitute the mobility term for an effective mobility μ_{eff} as shown in Eq. (20).

$$K_{dr,t}(V_m) = \frac{2\mu_{eff} V_{int,t}}{L^2}. (20)$$

Where $V_{int,t}$ follows Eq. (9) with $V_{oc,dir}$ replaced by $V_{oc,t}$. In presence of trapping and de-trapping processes, the effective band mobility (μ_{eff}) is determined by the ratio between free charges (n_f) and total charges ($n_f + n_t$) through [48]:

$$\mu_{eff} = \mu_0 \frac{n_f}{n_f + n_t}, (21)$$

where μ_0 is the trap-free mobility. At MPP, Eq. (21) becomes

$$\mu_{eff,m} = \mu_0 \frac{1}{1 + N_t N_c{}^{(1-\Delta)} n_{f,m}{}^{(\Delta-2)}}, (22)$$

Finally, we obtain the transport-to-recombination factor for tail state mediated recombination ($\Gamma_{m,t}$):

$$\Gamma_{m,t} = \frac{K_{dr,t}(V_m)}{K_{rec,t}(V_m)} = \frac{2\mu_0\left(V_{bi} - wV_{oc,t}\right)}{L^2 B_t N_t N_c{}^{(1-\Delta)}\left[n_{f,m}{}^{(\Delta-1)} + N_t N_c{}^{(1-\Delta)} n_{f,m}{}^{(2\Delta-3)}\right]}. \quad (23)$$

Note that we express $\Gamma_{m,t}$ as a function of $n_{f,m}$ for better readability, since $n_{f,m}$ is positively dependent on the light intensity (I). In Eq. (23), the numerator has a negative but weak dependence on light intensity such that the term in the denominator dominates the relationship between I and $\Gamma_{m,t}$. The first term in the square brackets of the denominator can only result in a negative dependence of $\Gamma_{m,t}$ on I (negative *FF-I* dependence) since the reaction order is always greater than one ($\Delta > 1$) and $n_{f,m}$ increases with light intensity. The second term in the denominator can however result in a positive dependence of $\Gamma_{m,t}$ on I (positive *FF-I* dependence) for values of $\Delta < 1.5$. This corresponds to characteristic trap energies of $E_t > 2k_BT$ (approximately 52 meV at 300 K). This result implies that the reaction order is critical to defining the *FF-I* behaviour, and devices with higher reaction orders close to 2 are less likely to have a positive *FF-I* relation. The balance of these terms is also determined by the balance of the normalized generation rate C_G to the trap-mediated rate coefficient B_t and the total trap density N_t to the effective density of band states N_c. Results from the analytical model using realistic parameters are presented in Section III.B.2.

III. MODEL RESULTS: ANALYTICAL VERSUS NUMERICAL

In this section, analytical model results of FF versus Γ_m are compared with numerical drift diffusion simulations performed using gpvdm [32,33]. Comparisons are carried out firstly at 1 Sun illumination, then over a range of different illumination intensities.

A. Comparison of the analytical and numerical models at 1 Sun illumination

We first performed calculations using the proposed analytical model (Eq. (10) and Eq. (23)) under 1 Sun using a large parameter space to obtain a comprehensive picture of the correlation between FF and $\Gamma_{m,dir}$, and between FF and $\Gamma_{m,t}$. Figure S3 and S5 show that there is minimal impact on the Γ_m $vs. I$ relation with different values of w. We therefore fix $w = 0.8$ for the remainder of the analysis. For direct recombination, the mobility (μ) and recombination constant (B_{dir}) were varied using ranges of [10^{-5}, 10^{-1}] cm^2 V^{-1} s^{-1}, and [10^{-20}, 10^{-8}] m^{-3} s^{-1}, respectively. In the case of trap-mediated recombination, the effective trap density and characteristic energy were varied (U_t^{exp}= [10^{15}, 10^{28}] m^{-3} eV^{-1} and E_t= [0.05, 0.15] eV). The results for the $\Gamma_{m,dir}$ calculated using Eq. (10) and $\Gamma_{m,t}$ using Eq. (23) are compared to FFs obtained from J-V curves calculated using gpvdm [32,33,62] in Fig. 2. We note that gpvdm has been validated against experimental data in the past. [33,63,64] Despite that for extreme low values of $\Gamma_{m,dir}$ FF goes down with $\Gamma_{m,dir}$, within commonly observed FF values in the range from 50% to 70%, we find that FF increases with Γ_m for both direct and trap-mediated recombination. This is a similar trend to that first observed by Koster et al. [29] This agreement supports the validity of our analytical model under 1 Sun illumination.

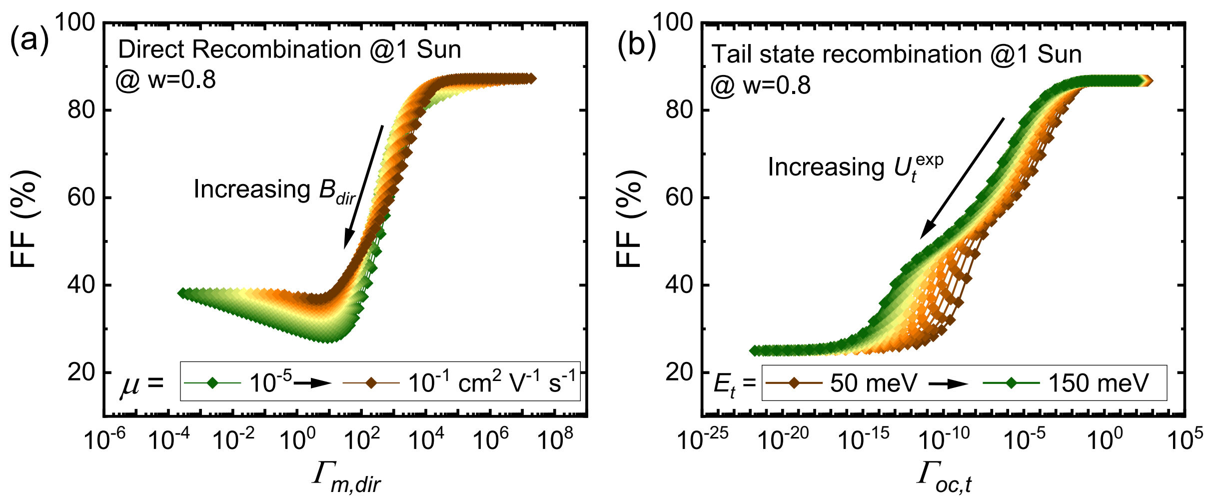

FIG. 2. FF as a function of Γ_m at 1 sun illumination with $w = 0.8$. (a) Direct recombination with varied bimolecular recombination constant (B_{dir} = [10^{-20}, 10^{-8}] m^{-3} s^{-1}) and mobility (μ = [10^{-5}, 10^{-1}] cm^2 V^{-1} s^{-1}). (b) Trap-mediated recombination with a varying characteristic energy (E_t= [0.05, 0.15] eV) assigned to the model along with trap densities (U_t^{exp}) varying from 10^{15} to 10^{28} m^{-3} eV^{-1}. The values are calculated at 1 Sun. 1000 data points, representing 1000 simulations are shown in each plot. *FF*s are calculated from simulated J-V curves in gpvdm, using the same sets of input parameters.

B. Comparison of the analytical and numerical models over a range of light intensities

1. *Direct recombination*

Figure 3(a) shows the correlation between $\Gamma_{m,dir}$ and light intensity (without any traps) based on the analytical model Eq. (10) with $w = 0.8$. Figures S4 and S6 show that different values of *w* produce similar trends and do not affect the main conclusions made in the analysis. $\Gamma_{m,dir}$ always shows negative dependence on the light intensity over a wide range of values of B_{dir}. The slope of the traces also remains constant, indicating that, for devices dominated by direct recombination, *FF* is expected to decrease with increasing light intensity. This result could explain the commonly observed *FF-I* relation in the literature. The input parameters are shown in Table S2 in the Supplemental Material [52]. Note that this analytical model relies on low mobility semiconductors. In the case of crystalline silicon solar cell, the transport is fast, the *FF* increases with increasing light intensity based on diode equation analysis [40]. We also find that in our drift-diffusion simulations, high mobility devices follow the ideal diode equations, while low mobility devices follow our analytical model, as shown in Fig. S2. A simple way to understand the effect of low mobility is to introduce a high transport (series) resistance in a diode model, and more discussion can be found in Section VI in the

Supplemental Material [52]. Therefore, the commonly observed negative *FF-I* relation in organic solar cells can be explained by the low-mobility induced transport resistance. While our analytical model cannot explain devices with ideal transport, it is useful for understanding devices based on low mobility materials ($\mu < 10^{-1}$ cm^2 V^{-1} s^{-1}).

The analytical results were also compared to *FF* values extracted from one-dimensional drift diffusion simulations of *J-V* curves over a range of light intensities and direct recombination coefficients ([10^{-19}, 10^{-11} m^{-3} s^{-1}]) using the same base parameter set (Table S3 of the Supplemental Material [52]) in gpvdm [32,33,62] (see Fig. 3b). The simulations confirm that *FF* decreases with increasing light intensity regardless of the value of B_{dir}. For low values of B_{dir} (<10^{-17} m^{-3} s^{-1}) , the slope of the *FF* versus light intensity curve is shallow and the value of *FF* tends to its upper limit as described by the Shockley-Queisser theory. [65] While the analytical model cannot reproduce this low B_{dir} limit, the agreement in trend between the analytical model and the drift-diffusion simulation results is good, at least for non-ideal solar cells with moderate recombination coefficients.

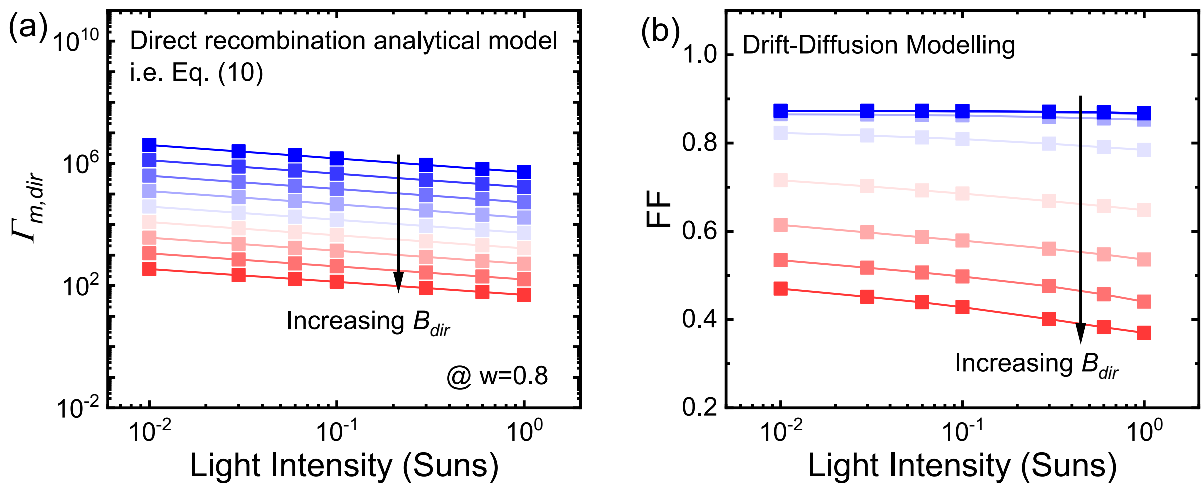

FIG. 3. Direct recombination: comparison between (a) $\Gamma_{m,dir}$ and light intensity using Eq. (10) with $w = 0.8$ and (b) Numerically calculated *FF* versus light intensity from one-dimensional drift-diffusion simulations using gpvdm. B_{dir} was varied from 10^{-19} to 10^{-11} m^{-3} s^{-1}.

2. Tail state-mediated recombination

The effect of tail states on the $\Gamma_{m,t}\ vs. I$ relation calculated using the expression given in Eq. (23) is shown in Fig. 4 (a-f). We vary two key variables for the calculations: the characteristic energy E_t, and the effective density of trap states U_t^{exp}. The characteristic energy has been reported to vary from 0.03 to 0.08 eV. [66–69] Here we compare low (0.03 eV), moderate (0.06 eV) and high (0.10 eV) characteristic energies with different effective tail state densities. Figure 4 (a-c) shows that E_t changes the mobility (μ_{eff}) - light intensity (I) dependence significantly. With a low characteristic energy ($E_t = 0.03\ eV$), μ_{eff} is largely unaffected by I, even with reasonably high effective trap densities (10^{24} m^{-3} eV^{-1}). By contrast, for larger characteristic energies, $E_t > 2k_BT$ ($E_t = 0.06\ or\ 0.10\ eV$), μ_{eff} is clearly reduced with increased U_t^{exp} and lower light intensity. Consequently, as described by Eq. (23), the $\Gamma_{m,t}\ vs. I$ relation is strongly affected by μ_{eff}. With low values of E_t, $\Gamma_{m,t}$ always shows a negative dependence on light intensity and the value of U_t^{exp} has little effect on the curve. With a high value of E_t, a clear change in the $\Gamma_{m,t}\ vs. I$ gradient with different values of U_t^{exp} is observed: the higher the value of U_t^{exp}, the more positive the slope of $\Gamma_{m,t}\ vs. I$ curve. These results clearly demonstrate that charge transport and recombination involving tail states can have a strong influence on the shape of the *FF-I* plot. The observed trend is attributable to the reduced effective charge transport mobility when trapping and de-trapping process are involved. The input parameters used in the analytical model are listed in Table I.

We also performed one-dimensional drift-diffusion simulations with an exponential distribution of trap states using gpvdm [32,33,62] and the *FFs* were calculated at different light intensities. A comparison of the results based on the same parameters as given in Table S3 are shown in Fig. 4 (g-l). Figure S7 shows the effect of capture cross sections on the *FF-I* relation; Values of the cross-section for capture of free to trapped electrons (holes) were chosen to ensure fast charge capture (trapping) rate, and hence traps to be active. The capture cross section of the conduction band tail is chosen to be at least three orders of magnitude higher for capture of electrons (trapping) relative to the capture cross sections for holes (recombination). For the valence band tail, this ratio is inverted with hole capture being more efficient than electron capture. Thereby, the conduction (valence) band tail is heavily populated with trapped electrons (holes) without the recombination rate being overwhelmingly high. The capture cross sections of holes (electrons) in the conduction (valence) band tail are, however, still high enough to ensure that recombination occurs primarily via tail states. The high ratio between trapping and recombination cross sections ensures that charge density is able to build up in the tail before recombining, leading to light intensity dependent effects such as the light intensity dependent mobility that is often seen in organic semiconductors [46,47].

With a low value of E_t ($30\ meV$), μ_{eff} at MPP does not show a notable variation with light intensity (Fig. 4 (g)). Simultaneously, the *FF* shows a continuous increase with reduced light intensity with a shallow gradient due to negligible recombination (Fig. 4 (j)). In this instance, the effect of traps density is negligible, provided the effective trap density (U_t^{exp}) is less than 10^{24} m^{-3} eV^{-1}. With higher values of E_t (0.06 or 0.10 eV) but low U_t^{exp} (10^{18} m^{-3} eV^{-1}), μ_{eff} at MPP remains unchanged with varied light intensity (Fig. 4 (h,i)), and *FF* shows a similar trend to the $E_t = 30$ meV case (Fig. 4 (k,l)). However, when U_t^{exp} is increased, μ_{eff} at MPP starts to decrease notably with reduced light intensity (Fig. 4 (h,i)) and the slope of *FF-I* plot switches from negative to positive with light intensity (Fig. 4 (k,l)). The decrease of μ_{eff} at MPP for devices with high E_t and U_t^{exp} is caused by the reduced free-to-total charge carrier ratio ($n_f/(n_t + n_f)$) at low light intensity relative to 1 Sun. Recall from Eq. (12), that we expect the carrier densities to depend on quasi-Fermi-level splitting like $n_t \propto exp\left(-\frac{\Delta E_F}{E_t}\right)$ and $n_f \propto$

$exp\left(-\frac{\Delta E_F}{k_B T}\right)$. At low light intensities below 1 Sun, n_t is much higher than n_f owing to the difference in the exponential terms when N_t is large and $E_t > k_B T$. In this situation, $n_f/(n_t + n_f)$ is very small. With increased light intensity, n_f increases at a faster rate than n_t, and at 1 Sun making the ratio $n_f/(n_t + n_f)$ much larger than at lower light intensities.

The effects of the effective mobility (μ_{eff}) on the *FF-I* relation can also be explained in terms of the relative recombination rate. Inefficient charge transport will result in a higher recombination rate at a given light intensity and voltage. It follows that, at low light intensity, the recombination rate relative to the generation rate at voltages less than V_{oc}, ($R(V)/G$) is expected to be higher than that under 1 Sun illumination. Figure 5 shows calculated $R(V)/G$ as a function of voltage for two devices that have different U_t^{exp} (10^{18} and 10^{22} m^{-3} eV^{-1}) but the same E_t (100 meV) using gpvdm. The devices show positive and negative *FF-I* relations for high and low U_t^{exp} respectively as shown in Fig. 4 (l). With low U_t^{eff} (Fig. 5 (a)), $R(V)/G$ at V_m is lower at low light intensity (0.01 Sun) relative to 1 Sun, indicating lower recombination, consistent with higher *FF*. However, with high U_t^{exp} (Fig. 5 (b)), at 0.01 Sun $R(V)/G$ is significantly higher than at 1 Sun across the range of scanned voltages, which suggests higher recombination rates and lower *FF* at $I = 0.01$ Sun. The analysis in terms of relative recombination rate is consistent with that based on the effective mobility.

These results based on numerical simulations using gpvdm are consistent with the observations from our analytical model. We have also ruled out the possibility that interfacial contact barriers at the electrodes could produce a positive *FF-I* dependence (see Section X in Supplemental Material for further details [52]). We conclude that the influence of tail states can theoretically account for different *FF-I* relationships. These results combined with Fig. 3 also show that our analytical models can be useful for both 1 Sun and light-intensity dependent analysis for *FF*.

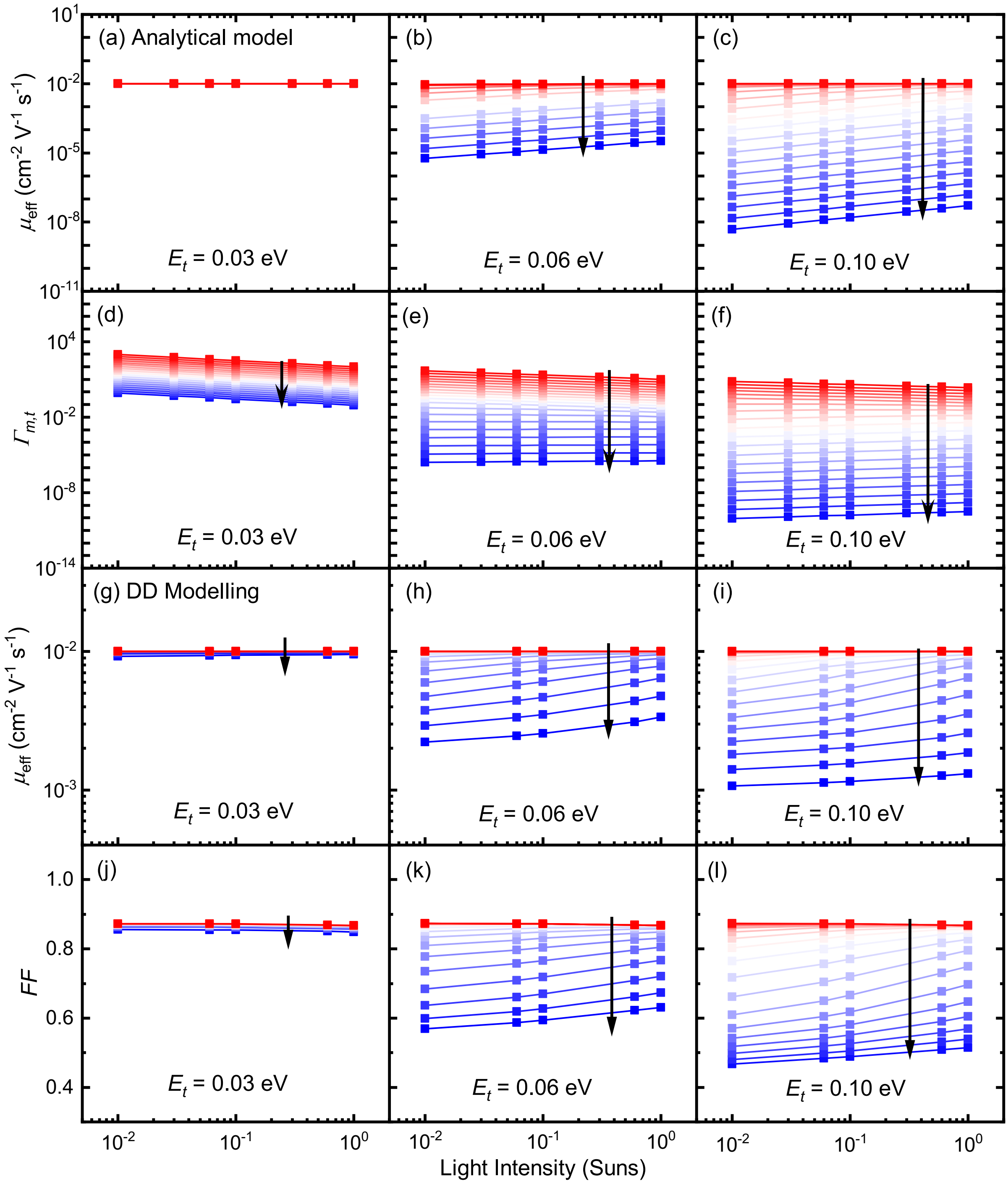

FIG. 4. Tail state-mediated recombination: analytical model Eq. (23) ($w = 0.8$) compared with numerical drift-diffusion simulation results. (a-c) Carrier mobility and (d-f) $\Gamma_{m,t}$ as a function of light intensity with respect to different effective trap densities for (a, d) low (0.03 eV), (b, e)

moderate (0.06 eV) and (c, f) high (0.10 eV) exponential characteristic energy (E_t) using analytical model Eq. (23). Drift diffusion simulation (gpvdm) results: (g-i) μ_{eff} at MPP and (j-l) FF as a function of light intensity for (g,j) low, (h,k) moderate and (i,l) high characteristic energy. The effective density of tail states U_t^{exp} was varied from 10^{18} to 10^{24} m^{-3} eV^{-1}, as shown from red to blue lines in the figures.

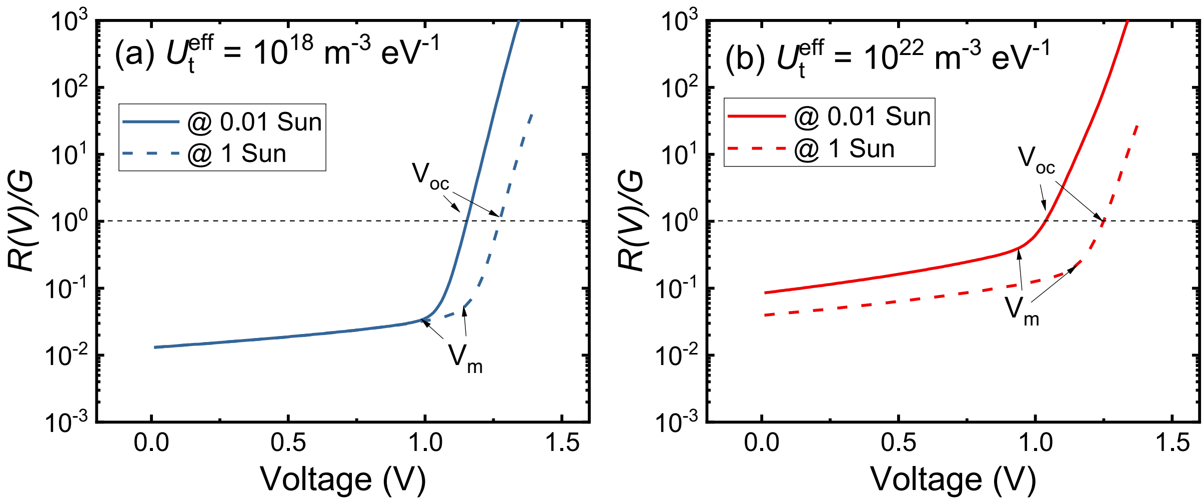

FIG. 5. Calculated relative recombination rate ($R(V)/G$) using gpvdm as a function of voltage for devices with (a) low (10^{18} m^{-3} eV^{-1}) and (b) high (10^{22} m^{-3} eV^{-1}) effective trap density (U_t^{exp}). E_t is set to be 100 meV.

TABLE I. Key input parameters for the analytical model Eq. (23).

Parameters	Symbol	Values	Units
Temperature	T	300	K
Effective density of states of free charges	N_C, N_V	1×10^{25}	m^{-3}
Active layer thickness	L	100	nm
Effective electron trap density per unit energy	U_t^{exp}	Varied	m^{-3} eV^{-1}
Exponential tail state DOS characteristic energy	E_t	Varied	eV
Trap-Free Mobility	μ_0	1×10^{-2}	cm^2 V^{-1} s^{-1}
Built-in Voltage	V_{bi}	1.6	V
Trap-mediated recombination coefficient	B_t	1×10^{-8}	m^3 s^{-1}
Generation rate at 1 sun	C_G	2×10^{28}	m^{-3} s^{-1}

Note: DOS = Density of states. V_{bi} follows effective band gap E_g, since we consider ideal Ohmic contact with no contact barriers. The choice of E_g or V_{bi} is made based on the recent development on novel non-fullerene acceptors [70–74]*, which often presents a E_g of 1.6 eV. We also note here that the FF-I relation is maintained regardless of the value of V_{bi} (see Figure S10 in the SI).*

IV. EXPERIMENTAL RESULTS

Having investigated the relationship between *FF* and light intensity theoretically, we now proceed to demonstrate the modelled *FF-I* behavior using practical organic solar cell devices.

A. Experimental *FF-I* relation

To investigate the *FF-I* relation of practical organic materials based solar cells, inverted architecture (Fig. 6(a)) OSCs based on PTB7-Th [34] as the donor, and either blended with the fullerene acceptor $PC_{71}BM$ or the non-fullerene acceptor O-IDTBR [35] were fabricated (see Experimental Section in the Supplemental Material [52] for more details regarding device fabrication). The energy level alignment of the studied materials [35,75–81] and contacts [82] is presented in Fig. S11 in the Supplemental Material [52]. Current density-voltage (*J-V*) curves for PTB7-Th:$PC_{71}BM$ and PTB7-Th:O-IDTBR devices under AM1.5 G simulated sunlight at different illumination intensities were measured with the resulting *FF-I* data shown in Fig. 6(b). Devices based on $PC_{71}BM$ and O-IDTBR showed completely different responses to the irradiation intensity under a simulated AM 1.5 G solar spectrum in terms of *FF*. For PTB7-Th:O-IDTBR devices, the *FF* increases with illumination intensity, while the *FF* of the PTB7-Th:$PC_{71}BM$ device has a negative dependence on the irradiation intensity, as previously seen in the literature [16–21].

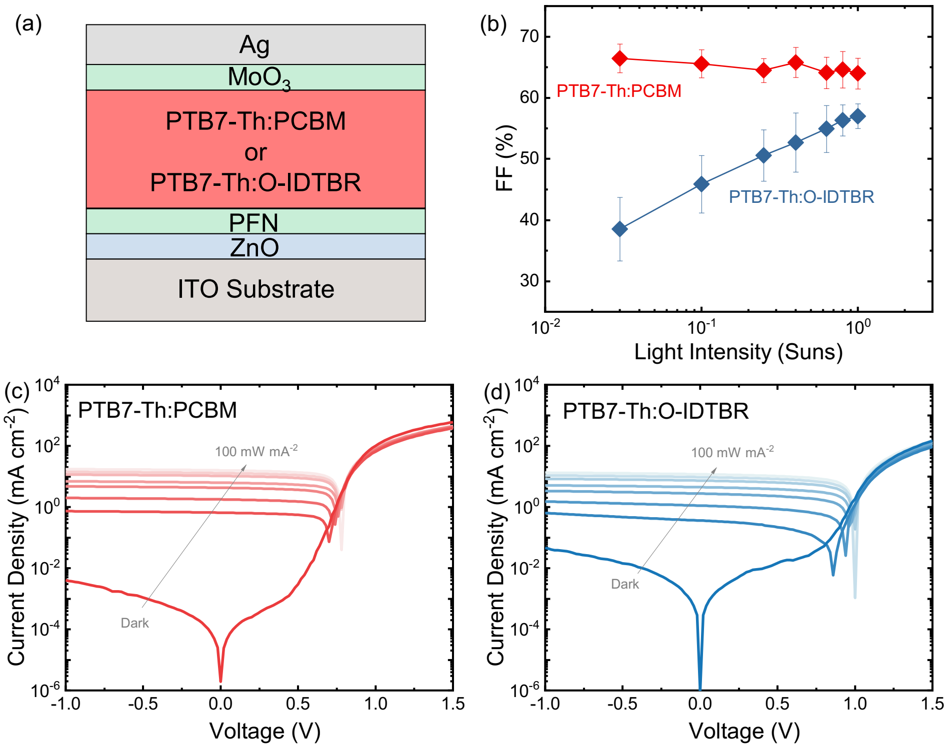

FIG. 6. Device structure, experimental *FF-I* results, and current density-voltage characteristics. (a) Inverted device structure for the organic solar cell fabrication: ITO/ZnO/PFN/PTB7-Th:$PC_{71}BM$ (1:1.5 ratio by mass, 80 ±5 nm) or PTB7-Th:O-IDTBR (1:1 ratio by mass, 80 ±5 nm)/MoO3/Ag; (b) Averaged fill factor with standard derivations as a function of light intensity as extracted from current density-voltage characteristics. At least three devices were measured for both the PTB7-Th:$PC_{71}BM$ and PTB7-Th:O-IDTBR architectures. Current density-voltage curves at different light intensities for (c) PTB7-Th:$PC_{71}BM$ and (d) PTB7-Th:O-IDTBR devices. A single representative device of each type is shown.

As the effect of leakage current has often been used to explain the *FF* reduction at low light intensity, [15,23] we first compared the dark current density with light current density at different illumination intensities, as shown in Fig. 6(c) and (d). Although the reverse dark current of $PC_{71}BM$ based device is around one order of magnitude lower than that of the O-IDTBR device, we find that the dark current for both devices is greater than one order of magnitude lower than the current density under the lowest light intensity (3 mW cm^{-2}). In addition, the reduction of *FF* for O-IDTBR devices becomes apparent at 1 Sun, where the current density is at least two order of magnitude higher than the dark current density suggesting the origin is unlikely to be the leakage current in this case. However, the fact that the O-IDTBR device presents higher reverse dark current than the $PC_{71}BM$ device is an indication that the O-IDTBR device suffers more recombination than the $PC_{71}BM$ device. The two devices provide contrasting examples to understand the factors that control the *FF-I* relation in organic disordered semiconductor based solar cells.

B. Quantifying trap states

We have shown that both the analytical and numerical (drift-diffusion) modelling results indicate that direct recombination cannot produce a positive dependence of *FF* on light intensity in low mobility semiconductor-based solar cells. Conversely, the existence of a significant density of exponential-type trap states can affect the *FF-I* relation in such a way that *FF* is reduced at lower light intensities. In this section we show that the different *FF-I* dependencies of the two devices studied can be directly related to their different trap state densities.

1. Ideality factors

Measurements of device ideality factors have frequently been used to indicate the degree of recombination via trap states in OSCs [57]. As derived in Eq. (17), higher ideality factors correspond to a greater proportion of recombination via trap states.

We extracted the ideality factor ($n_{id,l}$) of the measured devices using V_{oc} versus light intensity plot (*Suns*-V_{oc}), as shown in Fig. 7. The ideality factors calculated from the slope of the curve fits were 1.00 ± 0.10 and 1.60 ± 0.20, for the $PC_{71}BM$ and O-IDTBR devices, respectively. We also estimated the dark ideality factor $n_{id,d}$ using dark J-V curves, showing the same trend as $n_{id,l}$ (see Methods section and Fig. S12 in Supplemental Material for further details [52]).

The O-IDTBR device presents notably higher ideality factors (closer to 2) than the $PC_{71}BM$ device (close to 1), indicating that trap mediated recombination is likely to play a bigger role in the O-IDTBR devices than in the $PC_{71}BM$ devices.

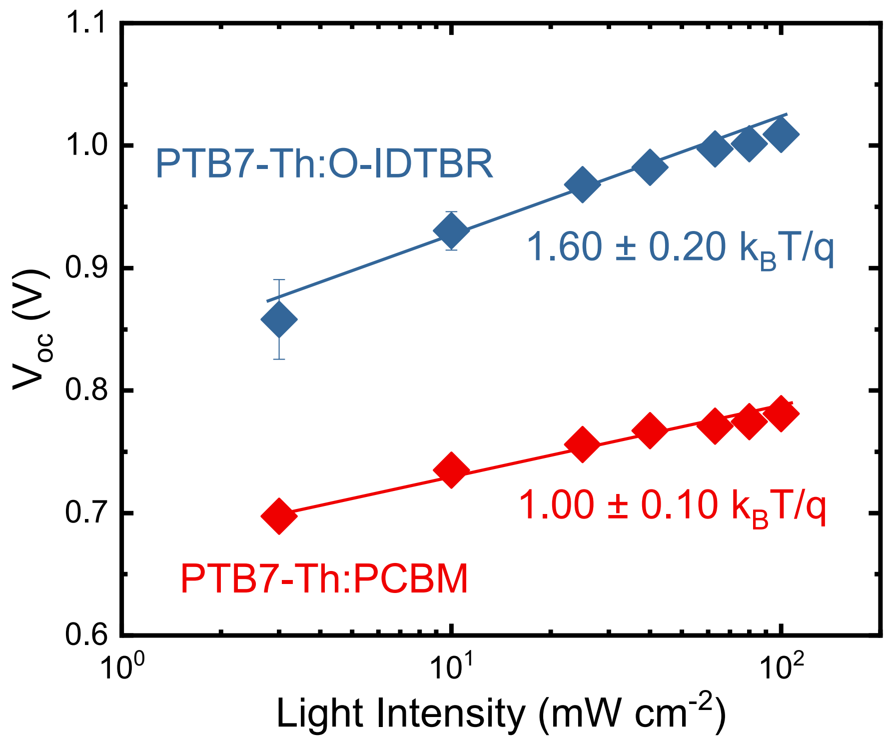

FIG. 7. Experimental measured ideality factors. Open circuit voltage (V_{oc}) versus light intensity (I). The solid lines are fits to the data indicated by diamond markers.

2. *Low frequency capacitance*

Ideality factor measurements indicate that the O-IDTBR device likely presents more trap-mediated recombination than the $PC_{71}BM$ device. In this section we directly measure the trap state density of devices using low frequency (10 kHz) capacitance measurements. [51,83–85] Since the measurement frequency approaches the time scale of trapping and de-trapping, trapped carriers can respond to the alternating internal electric field. It has previously been argued that an increase in capacitance at higher applied DC voltages can be attributed to trap-states mediating the charge distribution and transport, [51,83–85] suggesting that an extended density of trap states is the origin of the low frequency capacitance enhancement.

We have adapted this concept to understand the influence of illumination intensity on the low frequency capacitance within the multiple trapping and de-trapping model. In the low frequency regime studied, the effects of deep traps cannot be detected while shallow traps can be. Under low illumination, the trap states are not fully occupied, and carriers mostly fill the deep states. As such the de-trapping rate is low owing to its exponential dependence on trap depth (E_{depth}), via $\propto exp\,(-\frac{E_{depth}}{k_B T})$. Deeply trapped carriers therefore do not strongly influence carrier dynamics. With increased light intensity, however, the shallow states start to be filled. In this situation, the rate of de-trapping becomes significant such as to influence transport and result in an increase in the measured capacitance. [83] Hence, the enhancement of capacitance at high light intensity is an indication of trap-mediated charge dynamics. The effect of trapping is expected to be more pronounced with low internal field, where charge extraction is slow. Measuring the capacitance response at low frequency under a range of applied voltages is therefore a useful method to detect the shallow trap states.

Here we apply these concepts to our OPV devices and perform capacitance-voltage (C-V) measurements under 10 kHz frequency at different applied DC voltages starting from -2 V to 2 V. Figure 8(a) shows the capacitance measured using a 50 mV AC voltage set at 10 kHz for the $PC_{71}BM$ and the O-IDTBR based devices measured at various light intensities (from 1 Sun to the dark). On applying a negative bias of -2 V, the capacitance converges to the geometric capacitance. In this regime, the strong electric field under large negative applied bias efficiently removes carriers such that charge recombination, transport or redistribution caused by trapping and de-trapping is small and can hardly interfere the dynamics of charge carriers. With increased voltage, the electrostatic potential difference between the contacts drops, leading to reduced drift currents. From this point, trap states start to play an active role in mediating charge carrier transport processes resulting in the increased capacitance seen in Fig. 8 (a). Both $PC_{71}BM$ and O-IDTBR devices presented an increased capacitance with reduced internal field, indicating that trap-mediated transport exists in both devices. However, a clear magnitude difference between the O-IDTBR and $PC_{71}BM$ devices is observed. The capacitance at low internal field (corresponding to ~1.2 V voltage) caused by trapping and de-trapping of carriers shows a large enhancement relative to the capacitance at the high internal field at high light intensity, while the enhancement is lower for lower light intensities due to the deep depth of filled trap states in the case of the O-IDTBR devices. For the $PC_{71}BM$ devices, at low and high light intensity, the magnitude of capacitance enhancement from negative to positive voltage is similar but significantly smaller than that for O-IDTBR devices. This suggests that there are significantly more occupied trap states in the O-IDTBR device than those in the $PC_{71}BM$ devices.

According to Ref. [83], under low frequency and high light intensities, the capacitance caused by trapping and de-trapping processes gives information of the lower limit of the trap density corresponding to the shallow traps. Here, deeper trap states can only be probed at low frequency on the same order as their de-trapping rates. Assuming the additional capacitance at V close to V_{bi} is caused by trapped carrier being released to the mobility edges, the trap-charge density of accessible trap states can be estimated using Eq. (24). [83,86,87]

$$\frac{1}{C^2} \propto -\frac{2}{N_t \varepsilon q A^2} V, (24)$$

where ε is the dielectric constant, C is the capacitance, A is the device area, and V is the applied voltage.

We obtained the trap density by fitting ${}^{1}/_{C^2}$ $vs. V$ plots at 1 Sun over the voltage range close to V_{bi}, as shown in Fig. 8(b). The slope of ${}^{1}/_{C^2}$ $vs. V$ in the $PC_{71}BM$ device is significantly higher than that of the O-IDTBR device (comparing positive values), indicating that the trap density is much lower in the $PC_{71}BM$ device than in the O-IDTBR device. Using Eq. (24), we obtain values of 2.5×10^{22} m^{-3}, and 2.0×10^{23} m^{-3} for the $PC_{71}BM$ and the O-IDTBR device at 10 kHz, respectively. The exact values of the total trap density in the two devices are difficult to determine since it's hard to obtain clean signals at extremely low frequencies due to experimental system noise, and the trap densities estimated above can only be related to the accessible traps at 10 kHz frequency and under 1 Sun illumination. However, the higher trap density extracted from the capacitance-voltage analysis is strong evidence that the O-IDTBR device has a higher total trap state density than the $PC_{71}BM$ device.

To verify our conclusions from the capacitance measurement, we performed *C-V* simulations at 10 kHz with a 50 mV AC voltage under different light intensities (the same as experimental C-V measurements) using gpvdm [32]. These C-V simulations are fully time-resolved and no additional assumptions have been made such as linearization of the equations. Since we do not know the precise parameters e.g. trap profile and density in the real devices, we do not perform a fitting routine to the experimental *C-V* curves, but rather aim for qualitative agreement. The simulations were carried out at $E_t = 0.10\ eV$ with the same parameter set as list in Table S3. The built-in voltage was set to 1 V and zero field mobility was set to 1×10^{-3} $cm^2\ V^{-1}\ s^{-1}$. We compared low (10^{18} m^{-3} eV^{-1}) and high (10^{24} m^{-3} eV^{-1}) effective trap densities. As shown in Fig. 8(c), although the magnitude of calculated *C-V* characteristics are much higher than that of the measured C-V, the simulated device with high trap density shows a much larger capacitance enhancement than the device with low trap density when we increase the light intensity from dark to 1 Sun. This result is consistent with the prior theory [83], namely that traps have a strong influence on the capacitance signal under a low frequency AC voltage. We also calculated $^{1}/_{C^2}$ $vs.$ V characteristics at 1 Sun as shown in Fig. 8(d). A clear slope difference is observed between low and high trap density device, which is also qualitatively consistent with the experimental results. The good agreement between experiments and simulations strongly supports our conclusions that the O-IDTBR device has a higher trap state density than the $PC_{71}BM$ device.

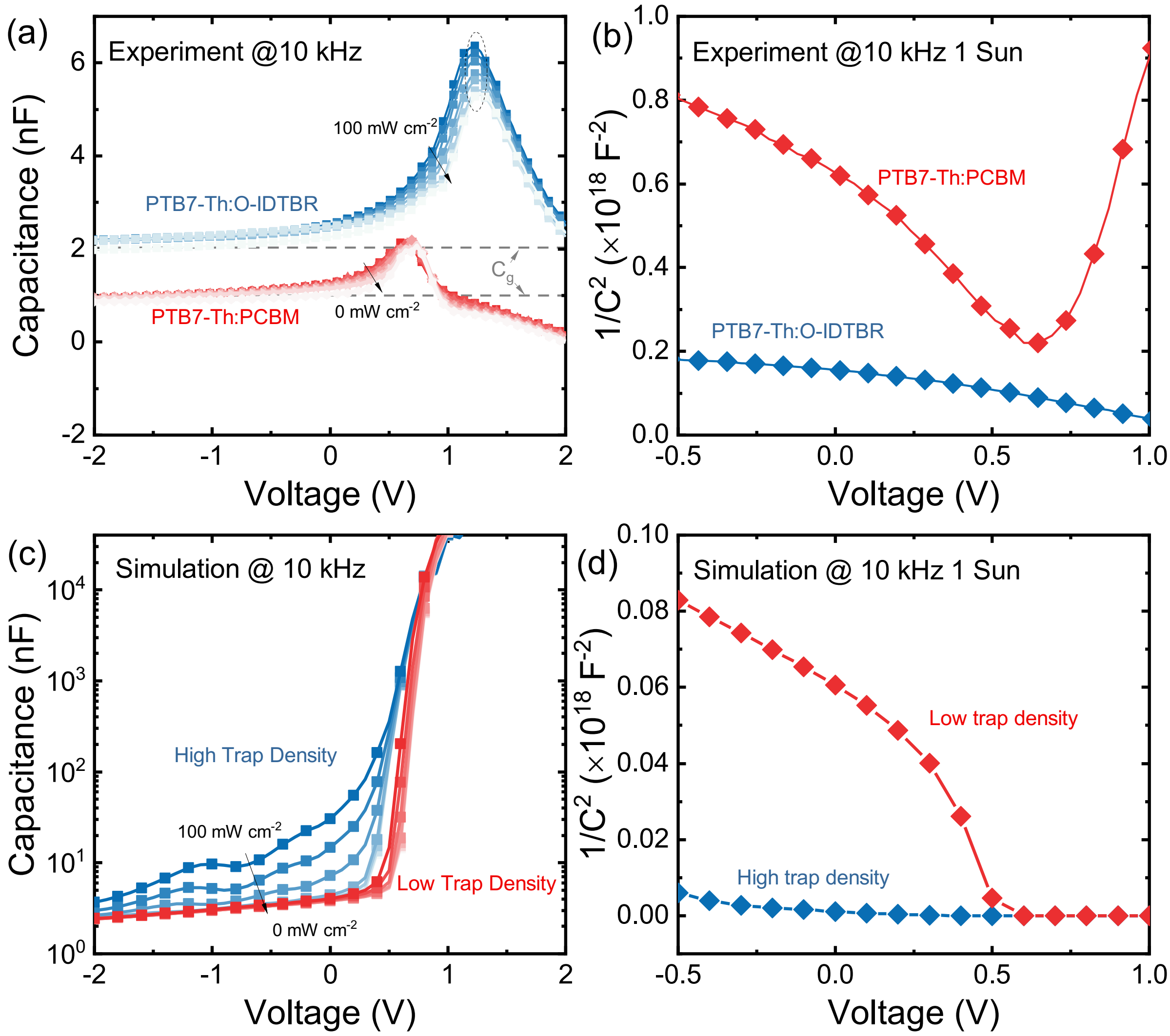

FIG. 8. Experimentally measured and simulated capacitance versus voltage characteristics. Experimental (a) $C\ vs.V$ characteristics at various light intensities and (b) $^{1}/_{C^2}\,vs.V$ characteristics at 1 Sun illumination under 10 kHz alternating voltage for PTB7-Th:$PC_{71}BM$

and PTB7-Th:O-IDTBR solar cells. Calculated (c) $C-V$ characteristics at different light intensities and (d) $1/_{C^2}$ $vs.V$ characteristics at 1 sun illumination under 10 kHz alternating voltage for simulated devices with low (10^{18} m^{-3} eV^{-1}) and high (10^{24} m^{-3} eV^{-1}) effective trap densities with the same characteristic energy for traps ($E_t = 0.10$ eV).

In summary, the O-IDTBR device presents a higher ideality factor, stronger trapping and de-trapping behaviour, and higher trap density than the $PC_{71}BM$ device. Consistent with our analytical model, the reduction of *FF* at low light intensity can be correlated to the existence of a significant density of tail states mediating carrier transport.

V. CONCLUSIONS

We proposed an analytical model parameterized by the transport-to-recombination factor Γ_m to help to understand the correlation between fill factor and light intensity in organic disordered semiconductor based solar cells. The analytical model suggests that, for low mobility devices that are limited by direct recombination, $\Gamma_{m,dir}$ always decreases with light intensity due to low mobility induced transport resistance. This accounted for the observed *FF-I* relation, where *FF* depends negatively on light intensity. For tail-state mediated transport and recombination, a positive dependence of $\Gamma_{m,t}$ on light intensity can be derived in cases where the characteristic energy (E_t) is greater than $2k_BT$ (52 meV at room temperature) resulting in a positive dependence of fill factor on light intensity. Charge density dependent carrier mobility caused by carrier trapping and de-trapping and a low reaction order are the principal origins of the positive *FF-I* relation. Our analytical models were verified using numerical drift-diffusion simulations (gpvdm) for both 1 Sun and light intensity dependent analyses.

To further verify the proposed analytical model, we characterized PTB7:$PC_{71}BM$ and PTB7-Th:O-IDTBR organic solar cells that showed negative and positive *FF-I* relation, respectively. Detailed experimental investigation showed that the O-IDTBR device had higher ideality factor, stronger carrier trapping and de-trapping behaviour, and a higher density of trap states than the $PC_{71}BM$ device. These experimental findings were consistent with the results from our analytical and numerical models indicating the importance of tail states in the analysis of light intensity dependence of fill factor in disordered semiconductor based solar cells.

The findings herein are particularly significant for devices that target low or high light-intensity applications such as indoor and concentrated photovoltaics. The conclusions can be extended from organic semiconductors to other disordered absorber materials. The analytical model provides a physical understanding of the relationship between fill factor and light intensity and the role played by tail states in this relation. It follows that measuring *FF-I* is a powerful technique to further characterize the density and nature of tail states in disordered semiconductor-based solar cell devices.

VI. ACKNOWLEDGEMENTS

J.N. and J.Y. thank the European Research Council for support under the European Union's Horizon 2020 research and innovation program (Grant Agreement No. 742708). P.C. and J.N. thank the UK Engineering and Physical Sciences Research Council (grant number EP/R020574/1) for financial support. Work in Jianghan University was financially supported by National Key R&D Program of China (2017YFB1104300), Project of Hubei Science and Technology Department (2019CFB198, 2019ZYYD005), and the Guiding Project of Education Department of Hubei Province (B2018259). The authors thank Qingzhong Zhou, Mingrui Zhang, and Feng Guo for experimental support, and Dr. Flurin D. Eisner, Dr. Piers R. F. Barnes, Mohammed Azzouzi, and William Fisher and for useful discussions.

REFERENCES:

[1] G. Li, R. Zhu, and Y. Yang, *Polymer solar cells*, Nat. Photonics **6**, 153 (2012).

[2] R. A. J. Janssen and J. Nelson, *Factors Limiting Device Efficiency in Organic Photovoltaics*, Adv. Mater. **25**, 1847 (2013).

[3] J. Nelson, *Polymer: Fullerene bulk heterojunction solar cells*, Mater. Today **14**, 462 (2011).

[4] A. J. Heeger, *25th Anniversary Article: Bulk Heterojunction Solar Cells: Understanding the Mechanism of Operation*, Adv. Mater. **26**, 10 (2014).

[5] J. Hou, O. Inganäs, R. H. Friend, and F. Gao, *Organic solar cells based on non-fullerene acceptors*, Nat. Mater. **17**, 119 (2018).

[6] J. Nelson, J. J. Kwiatkowski, J. Kirkpatrick, and J. M. Frost, *Modeling Charge Transport in Organic Photovoltaic Materials*, Acc. Chem. Res. **42**, 1768 (2009).

[7] J. Nelson, *The Physics of Solar Cells*, *The Physics of Solar Cells* (Imperial College Press, 2003).

[8] H. K. H. Lee, J. Wu, J. Barbé, S. M. Jain, S. Wood, E. M. Speller, Z. Li, F. A. Castro, J. R. Durrant, and W. C. Tsoi, *Organic photovoltaic cells – promising indoor light harvesters for self-sustainable electronics*, J. Mater. Chem. A **6**, 5618 (2018).

[9] Y. Cui, Y. Wang, J. Bergqvist, H. Yao, Y. Xu, B. Gao, C. Yang, S. Zhang, O. Inganäs, F. Gao, and J. Hou, *Wide-gap non-fullerene acceptor enabling high-performance organic photovoltaic cells for indoor applications*, Nat. Energy **4**, 768 (2019).

[10] S. R. Cowan, A. Roy, and A. J. Heeger, *Recombination in polymer-fullerene bulk heterojunction solar cells*, Phys. Rev. B - Condens. Matter Mater. Phys. **82**, 1 (2010).

[11] L. J. A. Koster, V. D. Mihailetchi, H. Xie, and P. W. M. Blom, *Origin of the light intensity dependence of the short-circuit current of polymer/fullerene solar cells*, Appl. Phys. Lett. **87**, 203502 (2005).

[12] A. K. K. Kyaw, D. H. Wang, V. Gupta, W. L. Leong, L. Ke, G. C. Bazan, and A. J. Heeger, *Intensity Dependence of Current–Voltage Characteristics and Recombination in High-Efficiency Solution-Processed Small-Molecule Solar Cells*, ACS Nano **7**, 4569 (2013).

[13] L. J. A. Koster, V. D. Mihailetchi, R. Ramaker, and P. W. M. Blom, *Light intensity dependence of open-circuit voltage of polymer:fullerene solar cells*, Appl. Phys. Lett. **86**, 123509 (2005).

[14] A. Maurano, C. G. Shuttle, R. Hamilton, A. M. Ballantyne, J. Nelson, W. Zhang, M. Heeney, and J. R. Durrant, *Transient optoelectronic analysis of charge carrier losses in a selenophene/fullerene blend solar cell*, J. Phys. Chem. C **115**, 5947 (2011).

[15] C. M. Proctor and T.-Q. Nguyen, *Effect of leakage current and shunt resistance on the light intensity dependence of organic solar cells*, Appl. Phys. Lett. **106**, 083301 (2015).

[16] C. M. Proctor, C. Kim, D. Neher, and T.-Q. Nguyen, *Nongeminate Recombination and Charge Transport Limitations in Diketopyrrolopyrrole-Based Solution-Processed Small Molecule Solar Cells*, Adv. Funct. Mater. **23**, 3584 (2013).

[17] L. H. Slooff, S. C. Veenstra, J. M. Kroon, W. Verhees, L. J. A. Koster, and Y. Galagan, *Describing the light intensity dependence of polymer:fullerene solar cells using an adapted Shockley diode model*, Phys. Chem. Chem. Phys. **16**, 5732 (2014).

[18] J. You, L. Dou, K. Yoshimura, T. Kato, K. Ohya, T. Moriarty, K. Emery, C.-C. Chen, J. Gao, G. Li, and Y. Yang, *A polymer tandem solar cell with 10.6% power conversion efficiency*, Nat. Commun. **4**, 1446 (2013).

[19] Y. Galagan, A. Manor, R. Andriessen, and E. A. Katz, *Analysis of light intensity dependence of organic photovoltaics: Towards efficient large-area solar cells*, in *2012 38th IEEE Photovolt. Spec. Conf.* (IEEE, 2012), pp. 002750–002752.

[20] A. Sharma, M. Chauhan, V. Bharti, M. Kumar, S. Chand, B. Tripathi, and J. P. Tiwari,

Revealing the correlation between charge carrier recombination and extraction in an organic solar cell under varying illumination intensity, Phys. Chem. Chem. Phys. **19**, 26169 (2017).

[21] C. G. Shuttle, R. Hamilton, B. C. O'Regan, J. Nelson, and J. R. Durrant, *Charge-density-based analysis of the current-voltage response of polythiophene/fullerene photovoltaic devices*, Proc. Natl. Acad. Sci. **107**, 16448 (2010).

[22] Y. Zhang, X.-D. Dang, C. Kim, and T.-Q. Nguyen, *Effect of Charge Recombination on the Fill Factor of Small Molecule Bulk Heterojunction Solar Cells*, Adv. Energy Mater. **1**, 610 (2011).

[23] Y. Zhou, T. M. Khan, J. W. Shim, A. Dindar, C. Fuentes-Hernandez, and B. Kippelen, *All-plastic solar cells with a high photovoltaic dynamic range*, J. Mater. Chem. A **2**, 3492 (2014).

[24] M. Stößel, J. Staudigel, F. Steuber, J. Blässing, J. Simmerer, and A. Winnacker, *Space-charge-limited electron currents in 8-hydroxyquinoline aluminum*, Appl. Phys. Lett. **76**, 115 (2000).

[25] P. E. Burrows, Z. Shen, V. Bulovic, D. M. McCarty, S. R. Forrest, J. A. Cronin, and M. E. Thompson, *Relationship between electroluminescence and current transport in organic heterojunction light-emitting devices*, J. Appl. Phys. **79**, 7991 (1996).

[26] R. S. Crandall, *Modeling of thin film solar cells: Uniform field approximation*, J. Appl. Phys. **54**, 7176 (1983).

[27] R. S. Crandall, *Transport in hydrogenated amorphous silicon p - i - n solar cells*, J. Appl. Phys. **53**, 3350 (1982).

[28] K. Hecht, *The mechanism of the primary photoelectric current in insulating crystals*, Z. Phys. **77**, 235 (1932).

[29] D. Bartesaghi, I. del C. Pérez, J. Kniepert, S. Roland, M. Turbiez, D. Neher, and L. J.

A. Koster, *Competition between recombination and extraction of free charges determines the fill factor of organic solar cells*, Nat. Commun. **6**, 7083 (2015).

[30] M. Stolterfoht, A. Armin, B. Philippa, and D. Neher, *The Role of Space Charge Effects on the Competition between Recombination and Extraction in Solar Cells with Low-Mobility Photoactive Layers*, J. Phys. Chem. Lett. **7**, 4716 (2016).

[31] P. Kaienburg, U. Rau, and T. Kirchartz, *Extracting Information about the Electronic Quality of Organic Solar-Cell Absorbers from Fill Factor and Thickness*, Phys. Rev. Appl. **6**, 1 (2016).

[32] R. C. I. MacKenzie, *General-purpose Photovoltaic Device Model—gpvdm*, Https://Www.Gpvdm.Com. (n.d.).

[33] R. C. I. MacKenzie, C. G. Shuttle, M. L. Chabinyc, and J. Nelson, *Extracting microscopic device parameters from transient photocurrent measurements of P3HT:PCBM solar cells*, Adv. Energy Mater. **2**, 662 (2012).

[34] Z. He, B. Xiao, F. Liu, H. Wu, Y. Yang, S. Xiao, C. Wang, T. P. Russell, and Y. Cao, *Single-junction polymer solar cells with high efficiency and photovoltage*, Nat. Photonics **9**, 174 (2015).

[35] D. Baran, R. S. Ashraf, D. A. Hanifi, M. Abdelsamie, N. Gasparini, J. A. Röhr, S. Holliday, A. Wadsworth, S. Lockett, M. Neophytou, C. J. M. Emmott, J. Nelson, C. J. Brabec, A. Amassian, A. Salleo, T. Kirchartz, J. R. Durrant, and I. McCulloch, *Reducing the efficiency-stability-cost gap of organic photovoltaics with highly efficient and stable small molecule acceptor ternary solar cells*, Nat. Mater. **16**, 363 (2017).

[36] A. Wadsworth, Z. Hamid, M. Bidwell, R. S. Ashraf, J. I. Khan, D. H. Anjum, C. Cendra, J. Yan, E. Rezasoltani, A. A. Y. Guilbert, M. Azzouzi, N. Gasparini, J. H. Bannock, D. Baran, H. Wu, J. C. de Mello, C. J. Brabec, A. Salleo, J. Nelson, F. Laquai, and I. McCulloch, *Progress in Poly (3-Hexylthiophene) Organic Solar Cells*

and the Influence of Its Molecular Weight on Device Performance, Adv. Energy Mater. **8**, 1 (2018).

[37] M. A. Green, *Solar cell fill factors: General graph and empirical expressions*, Solid. State. Electron. **24**, 788 (1981).

[38] C. van Berkel, M. J. Powell, A. R. Franklin, and I. D. French, *Quality factor in a -Si:H nip and pin diodes*, J. Appl. Phys. **73**, 5264 (1993).

[39] T. Kirchartz and J. Nelson, *Meaning of reaction orders in polymer:fullerene solar cells*, Phys. Rev. B **86**, 165201 (2012).

[40] K. Ruhle, M. K. Juhl, M. D. Abbott, and M. Kasemann, *Evaluating Crystalline Silicon Solar Cells at Low Light Intensities Using Intensity-Dependent Analysis of I–V Parameters*, IEEE J. Photovoltaics **5**, 926 (2015).

[41] N. H. Reich, W. G. J. H. M. van Sark, E. A. Alsema, R. W. Lof, R. E. I. Schropp, W. C. Sinke, and W. C. Turkenburg, *Crystalline silicon cell performance at low light intensities*, Sol. Energy Mater. Sol. Cells **93**, 1471 (2009).

[42] T. Kirchartz, J. Bisquert, I. Mora-Sero, and G. Garcia-Belmonte, *Classification of solar cells according to mechanisms of charge separation and charge collection*, Phys. Chem. Chem. Phys. **17**, 4007 (2015).

[43] S. J. Robinson, A. G. Aberle, and M. A. Green, *Departures from the principle of superposition in silicon solar cells*, J. Appl. Phys. **76**, 7920 (1994).

[44] T. C. M. Müller, B. E. Pieters, U. Rau, and T. Kirchartz, *Analysis of the series resistance in pin -type thin-film silicon solar cells*, J. Appl. Phys. **113**, 134503 (2013).

[45] D. Neher, J. Kniepert, A. Elimelech, and L. J. A. Koster, *A New Figure of Merit for Organic Solar Cells with Transport-limited Photocurrents*, Sci. Rep. **6**, 1 (2016).

[46] C. G. Shuttle, R. Hamilton, J. Nelson, B. C. O'Regan, and J. R. Durrant, *Measurement of Charge-Density Dependence of Carrier Mobility in an Organic Semiconductor*

Blend, Adv. Funct. Mater. **20**, 698 (2010).

[47] M. Bouhassoune, S. L. M. van Mensfoort, P. A. Bobbert, and R. Coehoorn, *Carrier-density and field-dependent charge-carrier mobility in organic semiconductors with correlated Gaussian disorder*, Org. Electron. **10**, 437 (2009).

[48] R. C. I. MacKenzie, T. Kirchartz, G. F. A. Dibb, and J. Nelson, *Modeling Nongeminate Recombination in P3HT:PCBM Solar Cells*, J. Phys. Chem. C **115**, 9806 (2011).

[49] T. Kirchartz, B. E. Pieters, J. Kirkpatrick, U. Rau, and J. Nelson, *Recombination via tail states in polythiophene:fullerene solar cells*, Phys. Rev. B - Condens. Matter Mater. Phys. **83**, 1 (2011).

[50] M. Kuik, L. J. A. Koster, G. A. H. Wetzelaer, and P. W. M. Blom, *Trap-assisted recombination in disordered organic semiconductors*, Phys. Rev. Lett. **107**, 1 (2011).

[51] L. Burtone, J. Fischer, K. Leo, and M. Riede, *Trap states in ZnPc:C60 small-molecule organic solar cells*, Phys. Rev. B **87**, 045432 (2013).

[52] *See Supplemental Material at [URL will be inserted by publisher] for experimental details, method section, derivation of key equations, as well as supporting figures and tables*.

[53] P. Das, *Maximum Power Tracking Based Open Circuit Voltage Method for PV System*, in *Energy Procedia* (Elsevier Ltd, 2016), pp. 2–13.

[54] S. M. Sze and K. K. Ng, *Physics of Semiconductor Devices*, *Physics of Semiconductor Devices* (John Wiley & Sons, Inc., Hoboken, NJ, USA, 2006).

[55] J. Yao, T. Kirchartz, M. S. Vezie, M. A. Faist, W. Gong, H. Wu, J. Troughton, T. Watson, and J. Nelson, *Quantifying losses in open-circuit voltage in solution processable solar cells*, Phys. Rev. Appl. **4**, 1 (2015).

[56] K. Tvingstedt and C. Deibel, *Temperature Dependence of Ideality Factors in Organic*

Solar Cells and the Relation to Radiative Efficiency, Adv. Energy Mater. **6**, 1502230 (2016).

[57] T. Kirchartz, F. Deledalle, P. S. Tuladhar, J. R. Durrant, and J. Nelson, *On the differences between dark and light ideality factor in polymer:Fullerene solar cells*, J. Phys. Chem. Lett. **4**, 2371 (2013).

[58] T. M. Burke, S. Sweetnam, K. Vandewal, and M. D. McGehee, *Beyond Langevin recombination: How equilibrium between free carriers and charge transfer states determines the open-circuit voltage of organic solar Cells*, Adv. Energy Mater. **5**, 1500123 (2015).

[59] J. Kniepert, I. Lange, N. J. van der Kaap, L. J. A. Koster, and D. Neher, *A Conclusive View on Charge Generation, Recombination, and Extraction in As-Prepared and Annealed P3HT:PCBM Blends: Combined Experimental and Simulation Work*, Adv. Energy Mater. **4**, 1301401 (2014).

[60] P. Mark and W. Helfrich, *Space-Charge-Limited Currents in Organic Crystals*, J. Appl. Phys. **33**, 205 (1962).

[61] J. A. Anta, J. Nelson, and N. Quirke, *Charge transport model for disordered materials: Application to Application to sensitized TiO2*, Phys. Rev. B **65**, 125324 (2002).

[62] N. Majeed, M. Saladina, M. Krompiec, S. Greedy, C. Deibel, and R. C. I. MacKenzie, *Using Deep Machine Learning to Understand the Physical Performance Bottlenecks in Novel Thin-Film Solar Cells*, Adv. Funct. Mater. **1907259**, 1907259 (2019).

[63] H. Mäckel and R. C. I. MacKenzie, *Determination of Charge-Carrier Mobility in Disordered Thin-Film Solar Cells as a Function of Current Density*, Phys. Rev. Appl. **9**, 34020 (2018).

[64] X. Shi, V. Nádaždy, A. Perevedentsev, J. M. Frost, X. Wang, E. von Hauff, R. C. I.

MacKenzie, and J. Nelson, *Relating Chain Conformation to the Density of States and Charge Transport in Conjugated Polymers: The Role of the β-phase in Poly(9,9-dioctylfluorene)*, Phys. Rev. X **9**, 021038 (2019).

[65] W. Shockley and H. J. Queisser, *Detailed Balance Limit of Efficiency of p-n Junction Solar Cells*, J. Appl. Phys. **32**, 510 (1961).

[66] S. A. Hawks, G. Li, Y. Yang, and R. A. Street, *Band tail recombination in polymer:fullerene organic solar cells*, J. Appl. Phys. **116**, 074503 (2014).

[67] R. A. Street, *Localized state distribution and its effect on recombination in organic solar cells*, Phys. Rev. B **84**, 075208 (2011).

[68] R. A. Street, A. Krakaris, and S. R. Cowan, *Recombination Through Different Types of Localized States in Organic Solar Cells*, Adv. Funct. Mater. **22**, 4608 (2012).

[69] J. Wu, J. Luke, H. K. H. Lee, P. Shakya Tuladhar, H. Cha, S.-Y. Jang, W. C. Tsoi, M. Heeney, H. Kang, K. Lee, T. Kirchartz, J.-S. Kim, and J. R. Durrant, *Tail state limited photocurrent collection of thick photoactive layers in organic solar cells*, Nat. Commun. **10**, 5159 (2019).

[70] J. Yuan, T. Huang, P. Cheng, Y. Zou, H. Zhang, J. L. Yang, S.-Y. Chang, Z. Zhang, W. Huang, R. Wang, D. Meng, F. Gao, and Y. Yang, *Enabling low voltage losses and high photocurrent in fullerene-free organic photovoltaics*, Nat. Commun. **10**, 570 (2019).

[71] Y. Cui, H. Yao, J. Zhang, T. Zhang, Y. Wang, L. Hong, K. Xian, B. Xu, S. Zhang, J. Peng, Z. Wei, F. Gao, and J. Hou, *Over 16% efficiency organic photovoltaic cells enabled by a chlorinated acceptor with increased open-circuit voltages*, Nat. Commun. **10**, 2515 (2019).

[72] C. Zhu, J. Yuan, F. Cai, L. Meng, H. Zhang, H. Chen, J. Li, B. Qiu, H. Peng, S. Chen, Y. Hu, C. Yang, F. Gao, Y. Zou, and Y. Li, *Tuning the electron-deficient core of a*

non-fullerene acceptor to achieve over 17% efficiency in a single-junction organic solar cell, Energy Environ. Sci. (2020).

[73] J. Zhang, W. Liu, M. Zhang, Y. Liu, G. Zhou, S. Xu, F. Zhang, H. Zhu, F. Liu, and X. Zhu, *Revealing the Critical Role of the HOMO Alignment on Maximizing Current Extraction and Suppressing Energy Loss in Organic Solar Cells*, IScience **19**, 883 (2019).

[74] C. Yang, J. Zhang, N. Liang, H. Yao, Z. Wei, C. He, X. Yuan, and J. Hou, *Effects of energy-level offset between a donor and acceptor on the photovoltaic performance of non-fullerene organic solar cells*, J. Mater. Chem. A **7**, 18889 (2019).

[75] L. Zhang, T. Yang, L. Shen, Y. Fang, L. Dang, N. Zhou, X. Guo, Z. Hong, Y. Yang, H. Wu, J. Huang, and Y. Liang, *Toward Highly Sensitive Polymer Photodetectors by Molecular Engineering*, Adv. Mater. **27**, 6496 (2015).

[76] Y. Zhang, D. Deng, K. Lu, J. Zhang, B. Xia, Y. Zhao, J. Fang, and Z. Wei, *Synergistic Effect of Polymer and Small Molecules for High-Performance Ternary Organic Solar Cells*, Adv. Mater. **27**, 1071 (2015).

[77] T. Jiang, J. Yang, Y. Tao, C. Fan, L. Xue, Z. Zhang, H. Li, Y. Li, and W. Huang, *Random terpolymer with a cost-effective monomer and comparable efficiency to PTB7-Th for bulk-heterojunction polymer solar cells*, Polym. Chem. **7**, 926 (2016).

[78] M.-A. Pan, T.-K. Lau, Y. Tang, Y.-C. Wu, T. Liu, K. Li, M.-C. Chen, X. Lu, W. Ma, and C. Zhan, *16.7%-efficiency ternary blended organic photovoltaic cells with PCBM as the acceptor additive to increase the open-circuit voltage and phase purity*, J. Mater. Chem. A **7**, 20713 (2019).

[79] L. Hu, W. Qiao, J. Qi, X. Zhang, J. Han, and C. Wang, *Significant enhancement of photodetector performance by subtle changes in the side chains of dithienopyrrole-based polymers*, RSC Adv. **6**, 22494 (2016).

[80] S. Holliday, R. S. Ashraf, A. Wadsworth, D. Baran, S. A. Yousaf, C. B. Nielsen, C. H. Tan, S. D. Dimitrov, Z. Shang, N. Gasparini, M. Alamoudi, F. Laquai, C. J. Brabec, A. Salleo, J. R. Durrant, and I. McCulloch, *High-efficiency and air-stable P3HT-based polymer solar cells with a new non-fullerene acceptor*, Nat. Commun. **7**, 1 (2016).

[81] S.-H. Liao, H.-J. Jhuo, Y.-S. Cheng, and S.-A. Chen, *Fullerene Derivative-Doped Zinc Oxide Nanofilm as the Cathode of Inverted Polymer Solar Cells with Low-Bandgap Polymer (PTB7-Th) for High Performance*, Adv. Mater. **25**, 4766 (2013).

[82] R. Xia, D. S. Leem, T. Kirchartz, S. Spencer, C. Murphy, Z. He, H. Wu, S. Su, Y. Cao, J. S. Kim, J. C. Demello, D. D. C. Bradley, and J. Nelson, *Investigation of a conjugated polyelectrolyte interlayer for inverted polymer:fullerene solar cells*, Adv. Energy Mater. **3**, 718 (2013).

[83] D. Ray, L. Burtone, K. Leo, and M. Riede, *Detection of trap charge in small molecular organic bulk heterojunction solar cells*, Phys. Rev. B **82**, 125204 (2010).

[84] L. Burtone, D. Ray, K. Leo, and M. Riede, *Impedance model of trap states for characterization of organic semiconductor devices*, J. Appl. Phys. **111**, 064503 (2012).

[85] P. P. Boix, G. Garcia-Belmonte, U. Muñecas, M. Neophytou, C. Waldauf, and R. Pacios, *Determination of gap defect states in organic bulk heterojunction solar cells from capacitance measurements*, Appl. Phys. Lett. **95**, 233302 (2009).

[86] J. D. Cohen and D. V Lang, *Calculation of the dynamic response of Schottky barriers with a continuous distribution of gap states*, Phys. Rev. B **25**, 5321 (1982).

[87] L. C. Kimerling, *Influence of deep traps on the measurement of free-carrier distributions in semiconductors by junction capacitance techniques*, J. Appl. Phys. **45**, 1839 (1974).